Title: Beyond the Volcano Limitations in Electrocatalysis – Oxygen Evolution Reaction

Authors: Niels Bendtsen Halck[a], Valery Petrykin[b], Petr Krtil[b*], Jan Rossmeisl[a*]

Supplementary Material:

Materials and Methods

The X-ray absorption spectroscopy (XAS) was used to gather information on local structures of the materials in the vicinity of both Ru, Ni and Co atoms. X-ray near edge absorption spectra (XANES) and extended X-ray absorption fine structure (EXAFS) data were collected on pellets containing 20-30 mg of $Ru_{1-x}Me_xO_2$ (Me= Co or Ni) in 200 mg of boron nitride (Aldrich, ACS grade) using X18B beam line (Si(111) monochromator) of the National Synchrotron Light Source (Brookhaven National Laboratory, USA). The spectra were measured in transmission mode at Ru K edge (22117eV) and Co and Ni K absorption edge (7709eV and 8333 eV, respectively). The Co and Ni K edge spectra of the sample with x= 0.05 were acquired in fluorescence mode using a 13 channel Ge detector. Each spectrum was recorded at three different scanning step sizes: pre-edge region from 200 to 30 eV was scanned in 5 eV steps to enable background subtraction; in the 30 eV pre-edge and 30 eV post-edge range the step size of 0.5 eV was used to acquire XANES part of the spectra, while the EXAFS data extending up to 16$Å^{-1}$ in the k-space were collected with the variable step size corresponding to 0.05 $Å^{-1}$.

The preliminary data handling, normalizations and extraction of the extended X-ray absorption fine structure (EXAFS) functions were performed in the IFEFFIT software package *(1)*. The photoelectron wave vector k for the Fourier transform of spectra was kept within the range of k=3.5-15.5$Å^{-1}$ for Ru-EXAFS and k=2-11.9$Å^{-1}$ for Co and Ni-EXAFS. The k-weighting factor of

2 was applied. The EXAFS functions were refined in R space in the range of R=1-6Å. The full-profile refinement of the EXAFS spectra by non-linear least squares (NLLS) minimization in the R-space with k-weighting factor equal to 2 was carried out using Artemis program of the IFEFFIT package. The theoretical models were generated using FEFF6.2 library.

Active site model formulation

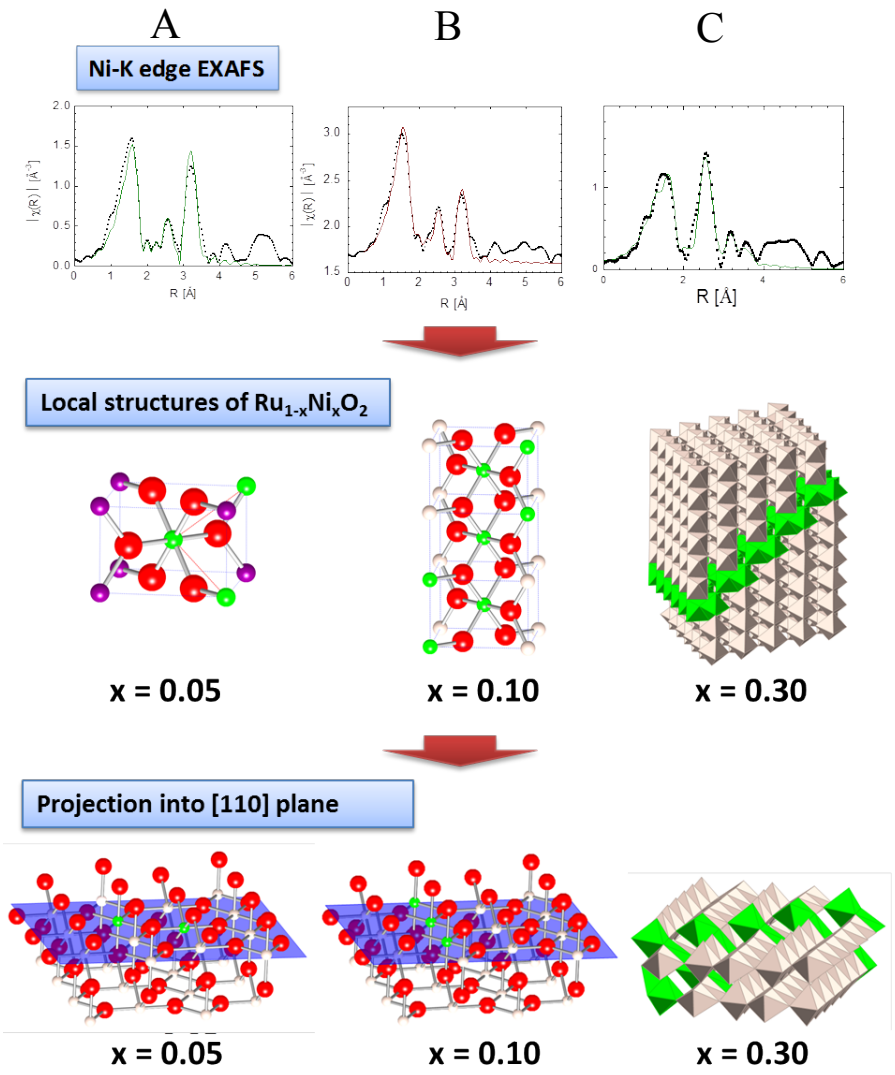

Figure 1S: Top layer shows typical EXAFS functions extracted from Ni K edge spectra of Ni modified ruthenia $Ru_{1-x}Ni_xO_2$ for three concentrations A) x = 0.05, B) x = 0.10 C) x = 0.3. The $Ru_{1-x}Ni_xO_2$-y phase shift is not compensated. The red lines show the NLLS fit used to estimate the occupancy of the cationic positions in the vicinity of the Ni ion. Middle layer shows corresponding local structures of the defects incorporated in the vicinity of the Ni ion. The bottom layer reflects the projection of the Ni ion confined defect to a {110} surface. The color coding of the atoms used in the structural models is as follows: oxygen – red,, ruthenium - grey, nickel – green.

Typ

ical

Ni K edge based EXAFS functions along with their refinement best fits are shown in Figure 1S. The schematic representation of the corresponding scattering events is presented to facilitate the active site model formulation. Relatively high symmetry of the rutile structural type allows assigning the individual maxima in observed EXAFS functions to individual metal-oxygen and metal – metal interactions. Particularly the metal-metal interaction signals are of importance since they allow to de-convolute the relative position of the doping cation (Ni, Co) with the majority cation (Ru) with respect to the catalytically important positions suggested in theoretical treatment of the oxygen evolution previously *(2)*. The refinement of the EXAFS data clearly outlines the tendency of the doping cations to cluster along the (111) direction of the rutile structure. While in the case of Co modified catalysts one finds the Co local environment concentration independent conforming to that shown in the left column of the Fig. 1S, in the case of Ni modified ruthenia one encounters a relatively complex clustering pattern with pronounced concentration dependence. The Ni modified ruthenia with the lowest Ni content shows exclusive Ni clustering along the (111) (Ni-Ni distance of 3.5Å) direction of rutile structure which gets complemented at higher Ni contents by the Ni-Ni clustering along (111) direction with that along (001) direction (Ni-Ni distance of 3.1 Å). The length of the Ni clusters running along the (001) direction (and consequently the size of the Ni cluster) increases with increasing Ni content. The Co modified ruthenia, on the other hand preserves the (111) compliant mode of cluster formation regardless of the total cobalt content. *(3,4)* Pronounced tendency of the doping cations to cluster along the body diagonal (i.e. along (111) vector) of the rutile elementary cell has significant consequences related to conceivable surface structures. The (111) vector stands out of the {110} planes which plays a pivotal role in the consideration of the rutile type oxides surfaces. The details of the refinement in terms of the quality of fit, boding distances, occupations and Debye

Waller factors were summarized for Ni and Co modified materials in references [17] and [18] of the main text, respectively

In this respect any Co (or Ni if the total Ni content remains sufficiently low) residing in surface position (regardless if *cus* or *bridge*) is free of in-surface Co or Ni neighbors. The nearest Co or Ni neighbors are residing below the surface.

This analysis allows formulating the defining structural elements shown in the Fig. 1 as the most representative modifications of the active site local structure on the {110} surfaces available for DFT modeling.

Oxygen evolution – theoretical model

The binding energies of the intermediates are calculated using density functional theory. The reaction mechanism for oxygen evolution on rutile 110 RuO_2 (ruthenia) *(2,6)* is shown below:

$$H_2O(l) + * \leftrightarrow HO^* + H^+ + e^- \quad (2)$$

$$HO^* \leftrightarrow O^* + H^+ + e^- \quad (3)$$

$$H_2O(l) + O^* \leftrightarrow HOO^* + H^+ + e^- \quad (4)$$

$$HOO^* \leftrightarrow * + O_{2(g)} + H^+ + e^- \quad (5)$$

* marks the active site which is a vacancy in the O covered *cus* row of Ru atoms. The binding energies for each step are calculated using the energies obtained from DFT relative to a RuO_2 with a vacancy for every two Ru ions and H_2O and H_2 in the gas phase

The Gibbs free energies are calculated from the binding energies obtained from DFT and including zero-point energy and entropy which are available in *(5)*. For HO, O and HOO zero

point energy and entropy amounts to 0.41, 0.05 and 0.46 eV, respectively. The theoretical over-potential is calculated by determining the step needing the highest potential to become downhill in free energy.

$$\Delta G_{HO*} = G_{HO*} - G_{*} - \left(G_{H_2O} - \frac{1}{2}G_{H_2}\right) \quad (6)$$

$$\Delta G_{O*} = G_{O*} - G_{*} - \left(G_{H_2O} - G_{H_2}\right) \quad (7)$$

$$\Delta G_{HOO*} = G_{HOO} - G_{*} - \left(2G_{H_2O} - \frac{3}{2}G_{H_2}\right) \quad (8)$$

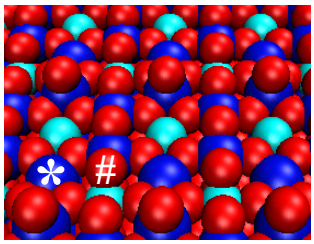

Figure 2S: Ni modified RuO_2 110 surface. The * marks the cus binding site and # the activated bridging O. Color code: Ru – blue, Ni – cyan and O – red.

The last step is the release of oxygen, the free energy of an oxygen molecule is set to 4.92 eV. This is to avoid the calculated energy of O_2 which is a well-known problem for DFT-GGA. The error on the energies of other intermediates relative to water is much smaller.

For the Ni modified RuO_2 surface the equations 2-5 are still valid from a stoichiometric point of view but since the O is activated due to the nearby Ni it acts as a proton acceptor creating two binding sites, one for oxygen species and one for protons. The corrected reaction mechanism is shown below where * denotes the active *cus* site and # describe the second active site which is the

bridge O next to Ni together with the relevant Gibbs free energies. The model system is depicted on figure 2S. An additional calculation is made for the Ni and Co modified ruthenia which is the energy of adding a proton to the bridging O site (#) (equation 13). The correction for zero-point energy and translational entropy is the difference between the correction for *OH and *O.

$$H_2O(l) + \ *\#\leftrightarrow O^* + H^\# + H^+ + e^- \quad (9)$$

$$O^* + H^\# \leftrightarrow O^* + H^+ + e^- \quad (10)$$

$$H_2O(l) + O^* \leftrightarrow OO^* + H^\# + H^+ + e^- \quad (11)$$

$$OO^* + H^\# \leftrightarrow *\# + \ O_2(g) + H^+ + e^- \quad (12)$$

$$\Delta G_{H^{\#}*} = G_{H^{\#}*} - G_* - \frac{1}{2}G_{H_2} \quad (13)$$

$$\Delta G_{H^{\#}O^*} = G_{H^{\#}O^*} - G_* - \left(G_{H_2O} - \frac{1}{2}G_{H_2}\right) \quad (14)$$

$$\Delta G_{\#_{O^*}} = G_{\#_{O^*}} - G_* - \left(G_{H_2O} - G_{H_2}\right) \quad (15)$$

$$\Delta G_{H^{\#}OO^*} = G_{H^{\#}OO^*} - G_* - \left(2G_{H_2O} - \frac{3}{2}G_{H_2}\right) \quad (16)$$

$$\Delta G_{\left(H^{\#}* + O_{2(g)}\right)} = G_{H^{\#}*} + G_{O_{2(g)}} - G_* - (2G_{H_2O} - \frac{3}{2}G_{H_2}) \quad (17)$$

The Gibbs free energy in equation 17 is determined using equation 13 and using $G_{O2(g)} = 4.92$ eV. The difference between equation 16 and 17 is whether the oxygen molecule is bound to the surface or not. This could be important as the oxygen molecule can leave the catalyst surface in either reaction 11 or 12. The energy difference is negligible in this case (see Table S1).

DFT results

The obtained Gibbs free energies from Dacapo *(6)* which used Vanderbilt pseudopotentials are compared to energies obtained from GPAW which uses real space grids and the projector-augmented wave method to treat core electrons *(7)*. For GPAW the 0.8.7929 setups were used. The systems treated, the 1x2 {110} RuO_2 surface and the 1x3 {110} for the Ni and Co modified ruthenia are identical and uses the same parameters but since the calculations are done on a real space grid there is no cutoff energies. Instead a grid spacing of 0.18Å is used. The comparison is listed in Table 1S.

Table 1S: Adsorptions energies for regular RuO_2 and Ni and Co modified RuO_2 with determination of the potential limiting step and the associated theoretical overpotential with two different DFT implementations, Dacapo (method 1) and GPAW (method 2).

	Method 1			Method 2		
	RuO_2	Ni modi. RuO_2	Co modi. RuO_2	RuO_2	Ni modi. RuO_2	Co modi. RuO_2
$\Delta G_{H^{\#}*}$ (eV)	--	-1.33	-1.23	--	-1.19	-1.18
$\Delta G_{H^{\#}O^*}$ (eV)	--	1.26	1.33	--	1.01	0.96
ΔG_{HO^*} (eV)	1.37	1.37	--	1.25	1.24	1.09
ΔG_{O^*} (eV)	2.73	2.75	2.59	2.34	2.29	2.19
$\Delta G_{H^{\#}OO^*}$ (eV)	--	3.57	3.62	--	3.68	3.61
$\Delta G_{\left(H^{\#}* + O_2(g)\right)}$(eV)		3.59	3.69		3.73	3.74
ΔG_{HOO^*} (eV)	4.38	4.45	---	4.11	4.27	4.06

Potential limiting step	$O^* \rightarrow HOO^*$	$H^{\#}O^* \rightarrow O^*$	$\# * \rightarrow H^{\#}O^*$	$O^* \rightarrow HOO^*$	$O^* \rightarrow H^{\#}OO^*$	$O^* \rightarrow H^{\#}OO^*$
Theoretical overpotential (V)	0.42	0.26		0.54	0.16	0.18

Doping with Ni or Co improves the catalytic activity of RuO_2 no matter the method due to stronger binding of hydrogenated species due to the splitting of these adsorbates on the surface and binding to the bridging O (#) and *cus* Ru (*). The binding of O to the cus site is not changed significantly by the Ni or Co doping. However, the binding of O to Ru is different for the two different implementations. This is most likely due to the different representations of the Ru core electrons.

The scaling between HO* and HOO* on oxides observed in literature *(7)* of 3.2 ± 0.2 eV is valid for regular RuO_2 using both methods and the scaling is broken with Ni or Co doping as the most stable configuration is O_2 and H# rather than HOO* which explains the position well above the apex of the volcano in Figure 5a of the manuscript.

References:

1. Ravel, B. & Newville, M. ATHENA, ARTEMIS, HEPHAESTUS: data analysis for X-ray absorption spectroscopy using IFEFFIT. *J. Synchrotron Radiat.* **12**, 537-541 (2005).
2. Hansen, H. A. *et al.* Electrochemical chlorine evolution at rutile oxide (110) surfaces. *Phys. Chem. Chem. Phys.* **12**, 283-290 (2010).
3. Petrykin, V., Macounova, K., Shlyakhtin, O. A. & P. Krtil, Tailoring the Selectivity for Electrocatalytic Oxygen Evolution on Ruthenium Oxides by Zinc Substitution. *Angew. Chem. Int. Ed.* **49**, 4813-4815 (2010).

4. Petrykin, V. *et al.*, Local Structure of Nanocrystalline Ru(1-x)Ni(x)O(2-delta) Dioxide and Its Implications for Electrocatalytic Behavior-An XPS and XAS Study. *J. Phys. Chem. C* **113**, 21657-21666 (2009).

5. Man, I. C. *et al.* Universality in Oxygen Evolution Electrocatalysis on Oxide Surfaces. *Chemcatchem* **3**, 1159-1165 (2011).

6. http://wiki.fysik.dtu.dk/dacapo

7. Enkovaara, J. *et al.*, Electronic structure calculations with GPAW: A real-space implementation of the projector augmented-wave method. *J. Phys.: Condens. Matter* **22**, 253202 (2010)